The mechanism of the glycosylase reaction with hOGG1 base-excision repair enzyme: concerted effect of Lys249 and Asp268 during excision of 8-oxoguanine

Jakub Šebera[1], Yoshikazu Hattori[2], Daichi Sato[3], David Řeha[4], Radim Nencka[1], Takashi Kohno[5], Chojiro Kojima[6,*], Yoshiyuki Tanaka[2,3,*] and Vladimír Sychrovský[1,7,*]

[1]The Institute of Organic Chemistry and Biochemistry, Academy of Sciences of the Czech Republic, Flemingovo náměstí 2, 166 10 Praha, Czech Republic, [2]Faculty of Pharmaceutical Sciences, Tokushima Bunri University, Nishihama-Boji 180, Yamashiro-cho, Tokushima 770 8514, Japan, [3]Graduate School of Pharmaceutical Sciences, Tohoku University, Aobayama, Sendai 980 8578, Japan, [4]Center for Nanobiology and Structural Biology, Institute of Microbiology, Academy of Sciences of the Czech Republic, v.v.i., Zámek 136, 373 33 Nové Hrady, Czech Republic, [5]Division of Genome Biology, National Cancer Center Research Institute 1-1, Tsukiji 5-chome, Chuo-ku, Tokyo 104 0045, Japan, [6]Graduate School of Engineering, Yokohama National University, Tokiwadai 79-5, Hodogaya-ku, Yokohama 240 8501, Japan and [7]Department of Electrotechnology, Electrical Engineering Czech Technical University, Technická 2, 166 27 Praha, Czech Republic

ABSTRACT

The excision of 8-oxoguanine (oxoG) by the human 8-oxoguanine DNA glycosylase 1 (hOGG1) base-excision repair enzyme was studied by using the QM/MM (M06-2X/6-31G(d,p):OPLS2005) calculation method and nuclear magnetic resonance (NMR) spectroscopy. The calculated glycosylase reaction included excision of the oxoG base, formation of Lys249-ribose enzyme–substrate covalent adduct and formation of a Schiff base. The formation of a Schiff base with $\Delta G^{\#} = 17.7$ kcal/mol was the rate-limiting step of the reaction. The excision of the oxoG base with $\Delta G^{\#} = 16.1$ kcal/mol proceeded via substitution of the C1′-N9 N-glycosidic bond with an H-N9 bond where the negative charge on the oxoG base and the positive charge on the ribose were compensated in a concerted manner by NH_3^+(Lys249) and CO_2^-(Asp268), respectively. The effect of Asp268 on the oxoG excision was demonstrated with ^{1}H NMR for WT hOGG1 and the hOGG1(D268N) mutant: the excision of oxoG was notably suppressed when Asp268 was mutated to Asn. The loss of the base-excision function was rationalized with QM/MM calculations and Asp268 was confirmed as the electrostatic stabilizer of ribose oxocarbenium through the initial base-excision step of DNA repair. The NMR experiments and QM/MM calculations consistently illustrated the base-excision reaction operated by hOGG1.

INTRODUCTION

The repair of damaged DNA is necessary to preserve genome integrity, and the damaged DNA bases are eliminated with the base-excision repair (BER) enzymes ([1–5]). The excision of the damaged base and scission of the DNA strand that involves abasic site are operated by bifunctional BER enzymes within the glycosylase and subsequent β-lyase reaction, respectively ([6]). The excision of the corrupted DNA base is the first irreversible step of the repair pathway that is initiated upon formation of the enzyme–DNA complex involving structural rearrangement of the corrupted DNA strand (Figure 1A) ([7–9]).

The primary factor leading to accumulation of DNA mutations is oxidative stress. oxoG, which arises from oxidatively damaged guanine (G) belongs to the most abundant and most dangerous DNA lesions (Figure 1B) ([10–12]). oxoG induces serious defects to organisms, and its continuous removal is crucial for the elimination of unwanted consequences of basal respiratory processes that normally occur in cells ([13]). By contrast, the controlled shutoff of oxoG
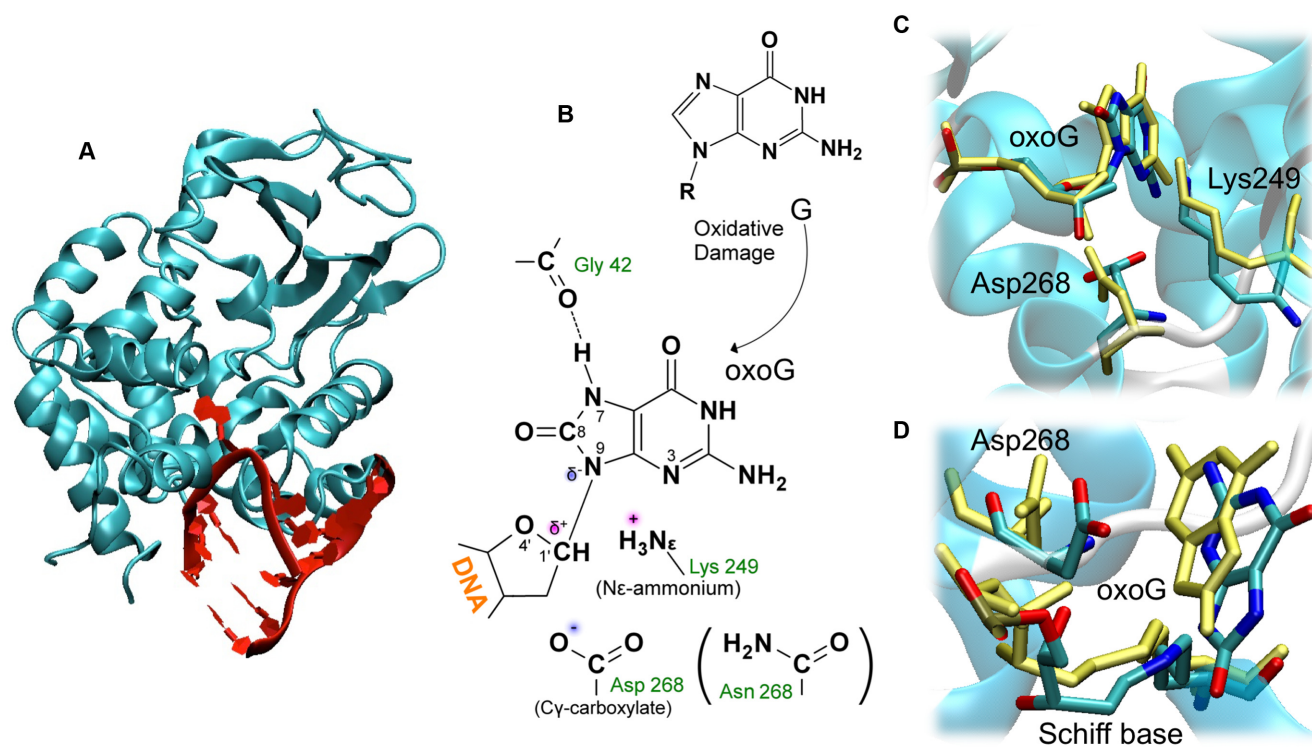
Figure 1. The hOGG1 BER enzyme. Sketch of the QM/MM structural model including hOGG1 (cyan) and oxoG-containing DNA (red) that was derived from the 2NOZ (33) crystal structure (**A**). The chemical structure of guanine (G), oxoG, Lys249 and Asp268 in WT hOGG1 and Asn268 in the hOGG1(D268N) mutant (**B**). Detail of the catalytic core before oxoG excision in 2NOZ (yellow) and in the QM/MM-optimized reactant (atom colored) (**C**). Detail of the catalytic core including Lys249-ribose covalent adduct with opened ring of sugar in the 1HU0 (34) crystal (yellow) and in the QM/MM-calculated reaction product (stationary state P+1) describing the Schiff base (atom colored) (**D**).

repair in cancer cells is assumed to be remedial in advanced anticancer therapies (14).

The glycosylase reaction operated by BER enzymes requires activation to surmount the energy barrier for cleavage of the N-glycosidic bond. The supply of up to 19 kcal/mol accelerates the bond cleavage 10^{14}-fold (4). All of the BER enzymes are typically lesion-specific which is particularly true for the hOGG1, which operates against oxoG with astonishing specificity (15–28). Misbehavior of hOGG1 most likely cannot occur, as a catalytic checkpoint prevents even scission of G forcibly inserted into the catalytic site (29). The insertion of oxoG into the catalytic site occurs much faster than the subsequent rearrangement of catalytic core (30). An inhibitor of hOGG1 that can mimic true substrates thus could become a therapeutic agent against certain types of cancer (31).

The structure of the hOGG1 catalytic core was disclosed by Verdine's group. First, they revealed the mechanistic basis for recognition and excision of oxoG using the inactive hOGG1(K249Q) mutant, where the Lys249 was substituted with Gln (8). Later, they demonstrated that Asp268 is another principal catalytic residue using the hOGG1(D268N) mutant where the Asp268 was substituted with Asn (Figure 1B) (32). These results led us to the focus on Lys249 and Asp268 in our work. Gly42, depicted also in the Figure 1B, is presumably responsible for recognition and proper deposition of oxoG within the catalytic core by the force of a hydrogen bond with H7(oxoG) (29).

The structure of the hOGG1 catalytic core, just before oxoG excision, was captured in the 2NOZ crystal (Figure 1C). Several glycosylase reaction mechanisms were assumed for different protonation states of Asp268 and Lys249 because the actual forms are currently unknown. CO_2^-(Asp268) was assumed to ensure electrostatic stabilization of the oxocarbenium cation on ribose during rupture of the N-glycosidic bond, as the mutation of Asp268 to Asn notably suppressed function of the hOGG1(D268N) mutant (32,35). As for Lys249, similar closeness of the Nε nitrogen to N3, N9 and C1′ atoms of oxoG (Figure 1B), observed in the crystals, indicated a variety of base-excision reactions. NH_3^+(Lys249) could stabilize the negative charge on the leaving oxoG base, whereas NH_2(Lys249) could stabilize the oxocarbenium cation on sugar. The respective base-excision reactions had actually been assumed (6,23,32,34,36,37). The mutation of Lys249 to Cys or Gln caused a loss of catalytic function of the bi-functional hOGG1 (8,34,37). Lys249 forms a Schiff base with the ribose of abasic site after oxoG excision (8). The Lys249-ribose covalent adduct, generated from the Schiff base upon the addition of a reducing agent, was captured in the 1HU0 crystal (34). Importantly, the geometries of the reactant and the product captured in the crystals can be used for reliable theoretical modeling of the glycosylase reaction (Figure 1C and D).

Compensation for the developing charges within a molecule of substrate by principal catalytic residues is a typ-

ical enzyme strategy (38). This general strategy was considered in theoretical calculations of the base-excision reactions operated by hOGG1 in a number of studies. The effect of NH_2(Lys249) on the oxocarbenium cation of ribose was compared with the effects of other nucleophiles (39,40). The cascade migration of the proton from NH_3^+(Lys249) to O8(oxoG) and then to O4′ of ribose activated the opening of the ribose ring and excision of the oxoG base (41). The synchronous attack of NH_2(Lys249) to C1′(ribose) and CO_2H(Asp268) to O4′(ribose) resulted in an opened ring of the oxoG ribose and subsequent excision of the oxoG base (the Ribose-protonated mechanism) (42). A similar mechanism was proposed for the opening of the sugar ring of a substrate nucleoside with endonuclease III-DNA (43). The π–cation interaction between the aromatic ring of the oxoG base and NH_3^+(Lys249) initiated proton transfer from NH_3^+(Lys249) to N3(oxoG), which activated the base-excision reaction (44,45). Lastly, the abstraction of the proton from NH_3^+(Lys249) with the N9(oxoG) atom triggered substitution of the N-glycosidic bond of oxoG with the N9-H bond in a concerted synchronous manner (the σ-bond substitution mechanism) (46).

The previous studies clearly demonstrate the principal effect of Lys249 and Asp268 on the catalytic function of hOGG1. As mentioned, protonation states of the two residues are presently unknown, and the function of these residues during the glycosylase reaction is therefore obscure. Nevertheless, typical pKa values for the Lys and Asp side-chains implicate likely NH_3^+(Lys249) and CO_2^-(Asp268) forms (47). Under this assumption, Lys249 presumably compensates for the negative charge on the leaving oxoG base and Asp268 compensates for the incipient charge on the ribose oxocarbenium. The σ-bond substitution reaction that complies with these assumptions was proposed previously, assuming only the effect of Lys249 (46). In the current work, the base-excision reaction with hOGG1 will be illustrated within a complete catalytic core by employing the QM/MM calculation method. The function of Asp268 will be particularly addressed. The Asp residue is known to be well-conserved with within the OGG family of BER enzymes; however, the function is still not clear (4). The nuclear magnetic resonance (NMR) measurements employing WT hOGG1 and the hOGG1(D268N) mutant in this work determined which of the functions of the bifunctional hOGG1 is actually affected by the D268N mutation. The NMR experiments and QM/MM calculations provided a coherent picture of the base-excision reaction within the glycosylase reaction operated by the hOGG1 BER enzyme.

MATERIALS AND METHODS

Experimental

The expression of WT hOGG1 and hOGG1(D268N). The cDNA encoding hOGG1 (12–327) was cloned into the multiple cloning site of pET47b vector (Novagen) and the D268N mutation was introduced by polymerase chain reaction. The resulting plasmids were used to transform *Escherichia coli* Rosetta (DE3) cells (Novagen), which were then grown in Luria Bertani (LB) medium until the cell suspension reached the appropriate turbidity. Chimeric proteins comprising His_6-tag fused to the N-terminus of hOGG1 or its mutants were then overexpressed by the addition of 1 mM isopropyl 1-thio-β-D-galactopyranoside for 24 h at 16°C, after which the cells were harvested by centrifugation. The overexpressed His_6-tagged hOGG1 proteins were initially purified by affinity chromatography using Ni-NTA resin (QIAGEN). After enzymatic cleavage of the His_6-tag from target proteins using GST-HRV 3C protease, the hOGG1 and mutant proteins were further purified by size exclusion column chromatography using Superdex 75 (GE Healthcare).

The preparation of oxoG-containing DNA duplex. The DNA oligomers were synthesized and purified, based on established methods (48–51). Reagent for incorporation of oxoG nuleoside into a DNA oligomer was purchased from Glen Research (8-oxo-dG-CE Phosphoramidite, # 10-1028-02). The sequences of the DNA oligomers were as follows:

Strand-1: 5′ d[GGCTTCATCGTTATT(oxoG)ATGACCT GGTGGATACCG] 3′
Strand-2: 5′ d[CGGTATCCACCAGGTCATCAATAA CGATGAAGCC] 3′

where (oxoG) represents the oxoG residue. These two strands were mixed at 1:1 ration to form the oxoG-containing DNA duplex.

The in vitro assay of hOGG1 catalytic activity. In vitro assays of WT and D268N mutant hOGG1 were performed under the solution containing 50 mM Tris–HCl (pH7.4), 50 mM NaCl, 2 mM ethylenediaminetetraacetic acid, 100 mg/ml bovine serum albumin, 3.33 μM hOGG1 protein and 1.67 μM DNA oligomer. Time-course of the reaction was traced at 0, 10, 30, 60 and 120 min. The result analyzed by using the 20% denaturing polyacrylamide gelelectrophoresis (PAGE) (acrylamide:N,N′-methylenebis(acrylamide) = 19:1) containing 8 M urea was visualized with SYBR Gold (Invitrogen).

The NMR measurements and monitoring of time-course of hOGG1 catalysis. A total of 40 μM of the protein, WT hOGG1 or hOGG1(D268N) mutant, was mixed with 0.5 mM oxoG-containing DNA duplex in a buffer of 50 mM Tris(-D11)–HCl (pH 7.5), 100 mM NaCl and 1 mM dithiothreitol. The DNA solution in the absence of protein contained 0.5 mM oxoG-containing DNA duplex in a buffer of 50 mM Tris(-D11)–HCl (pH 7.5), 100 mM NaCl and 1 mM dithiothreitol. The ^1H NMR monitoring of catalytic reaction was carried out with Bruker Ascend 500 MHz spectrometer at 293 K. For each spectrum, 1024 scans were accumulated, resulting in experimental time of 1 h. The measurement was repeated 20 times to obtain the time course of hOGG1 catalysis.

The HSQC NMR measurements of hOGG1 and hOGG1(D268N). The solution for ^1H-^{15}N heteronuclear single quantum correlation (HSQC) spectrum contained 150 μM uniformly ^{15}N-labeled hOGG1 WT or D268N, 20 mM sodium phosphate (pH 6.8) and 50 mM NaCl. The ^1H-^{15}N HSQC spectra were measured using a Bruker Avance-III HD 600 MHz spectrometer equipped with a cryogenic probe at 298 K.

The QM/MM calculations

The structural model was derived from the 2NOZ X-ray structure keeping explicit hydration of the catalytic core (33). The M06-2X (52) DFT functional with 6–31G(d,p) basis set (53) and OPLS2005 all-atom force field (54) were used for calculations of QM and MM parts, respectively. The Jaguar 8.2 (55,56) (QM part), Impact 6.1 (57) (MM part) and QSite 6.1 (58,59) calculation programs were employed in QM/MM calculations. The Fukui function, F^2, describing the electrophilic or nucleophilic character of atoms was calculated with QSite (60–62). The QM part included oxoG, Lys249 and Asp268 (65 atoms), and in some calculations also Gly42 (74 atoms excluding the hydrogen-atom caps in total). The intermediate states along the catalytic reaction were calculated as geometrical scans of respective reaction coordinates followed by subsequent unconstrained geometrical optimizations. The transition states were calculated by employing the Quadratic Synchronous Transit method. Validity of all the stationary states was checked with the vibration frequency calculation. The electrostatic and steric effects on the QM part were described by explicit protein–DNA environment within the MM part. The Gibbs free energies included the harmonic vibration corrections ($T = 298.15$ K and $P = 101325$ Pa) calculated for the QM part ended by hydrogen-atom caps. Detailed descriptions of the structural model and QM/MM calculations can be found in the Supporting Theoretical Section in the Supporting Information.

RESULTS

The QM/MM calculation of the glycosylase reaction with hOGG1

Lys249 and Asp268 are apparently directly involved in the catalytic reaction because their mutation considerably affected the function of hOGG1 (8,32,34,35,37). The protonation states of the two residues basically define their roles during the removal of the oxoG base. The typical pKa values of the Lys and Asp side-chain residue are 10.4 and 3.9, respectively (47). Similar pKa values were also calculated for Lys249 and Asp268 in both the original and geometry-optimized 2NOZ structure (Supplementary Table S1). These pKa values implicate the prevalence of the NH_3^+(Lys249) and CO_2^-(Asp268) forms that are prerequisites for the σ-bond substitution base-excision reaction (46).

The 2NOZ crystal structure unveiled the geometry of the hOGG1 catalytic core just before oxoG excision (33). The corrupted DNA base was found to be extruded out of the DNA duplex and deposited within the catalytic site (Figure 1A). The QM/MM geometry optimization of 2NOZ preserved mutual positioning of Lys249 and oxoG; however, the carboxylate group of Asp268 rotated and departed little from oxoG (Figure 1C). In fact, similar conformations of Asp268 in available X-ray structures illustrated flexibility of the residue within the catalytic site (Supplementary Figure S1).

The initial attack of lone-pair electrons at the N9(oxoG) to the ammonium $N\epsilon H_3^+$ group of Lys249 triggers the σ-bond substitution reaction (46). The distance between the N9(oxoG) and Nε(Lys249) atoms in 2NOZ and in the

QM/MM-optimized reactant was 3.027 and 2.969 Å, respectively. The attack of lone-pair electrons from N9(oxoG) to NH_3^+(Lys249) induced pyramidal geometry of the N9 atom (κ′ = 21.7°, Supplementary Table S2). The N9-pyramidalization of oxoG was clearly induced by residues within the catalytic core, because the geometry of the N9 atom of the free non-interacting oxoG nucleoside is planar (κ′ = 0°) (63). The distorted oxoG substrate calculated for the reactant state was thus oriented into a productive arrangement, with respect to initiation of the σ-bond substitution reaction.

The elongation of the N-glycosidic bond of the oxoG nucleoside resulted in the spontaneous transfer of a proton from NH_3^+(Lys249) to N9(oxoG); the C1′–N9 bond was readily substituted with a H–N9 bond (TS1 and IS1 stationary states, Figure 2). The Gibbs free activation energy, $\Delta G^\#$, calculated for oxoG excision was 16.1 kcal/mol and the Gibbs free reaction energy ΔG_R was 6.3 kcal/mol (Figure 3). Stability of the Gibbs free energies with respect to explicit hydration was demonstrated for the R, TS1 and IS1 states. Complete explicit hydration of the catalytic site was developed on top of already included x-ray resolved hydration in the 2NOZ (Supplementary Data, Structural Model, Supplementary Tables S2–4). The $\Delta G^\#$ and ΔG_R calculated for OxoG excision with the hydrated 2NOZ structural model was 15.9 and 5.5 kcal/mol, respectively. After rearrangement of the cleaved oxoG base (TS2), calculations continued towards the Schiff base where the Lys249–ribose covalent adduct formally involves the Nε–C1′ double bond. First, the Lys249–ribose adduct involving the Nε−C1′ single bond was calculated, upon shortening the C1′-Nε distance (TS3, $\Delta G^\# = 16.2$ kcal/mol). Only here, NH_2(Lys249) acted on the ribose oxocarbenium as nucleophile as was already assumed in the unified catalytic mechanism for DNA glycosylases by Llyod (6). Then, the proton at Nε(Lys249) was abstracted with CO_2^-(Asp268) (TS4) and transferred to the N3(oxoG) atom (TS5). Though nipped, the protonated oxoG base further worked as an enzyme cofactor and activated the opening of the ribose ring that resulted in formation of the Schiff base, as was previously proposed by Verdine (34) and calculated by Garavelli (45). The opening of the ribose ring was activated by the hydrogen bond between the H9(oxoG) and O4′(ribose) atoms (TS6, $\Delta G^\# = 17.7$ kcal/mol). The proton at N9(oxoG) spontaneously transferred to O4′(ribose) while the ring of ribose was opened. The transfer of the proton from N3(oxoG) to CO_2^-(Asp268) (TS7) resulted in the spontaneous transfer of a proton from the Nε atom of the Schiff base to N9(oxoG), which stabilized the product, P ($\Delta G_R = -14.7$ kcal/mol). The C1′-Nε bond in P was formally a double bond (C1′-Nε = 1.265 Å), whereas that in 1HU0 crystal was a single bond owing to the borohydrate additive (C1′-Nε = 1.459 Å) (34). Moreover, the distance between O4′(ribose) and the O atom of CO_2^-(Asp268) calculated for the P (3.188 Å) was longer than the distance in 1HU0 (2.863 Å). The respective rearrangement of the catalytic core that complied better with 1HU0 [O4′(ribose)-O(Asp268) = 2.698 Å] resulted in further stabilization of the product, P+1 ($\Delta G_R = -10.8$ kcal/mol). The geometry of P+1 was consistent with the geometry in 1HU0 (Figure 1D). The QM/MM reaction pathway linked two principal states of the glycosy-
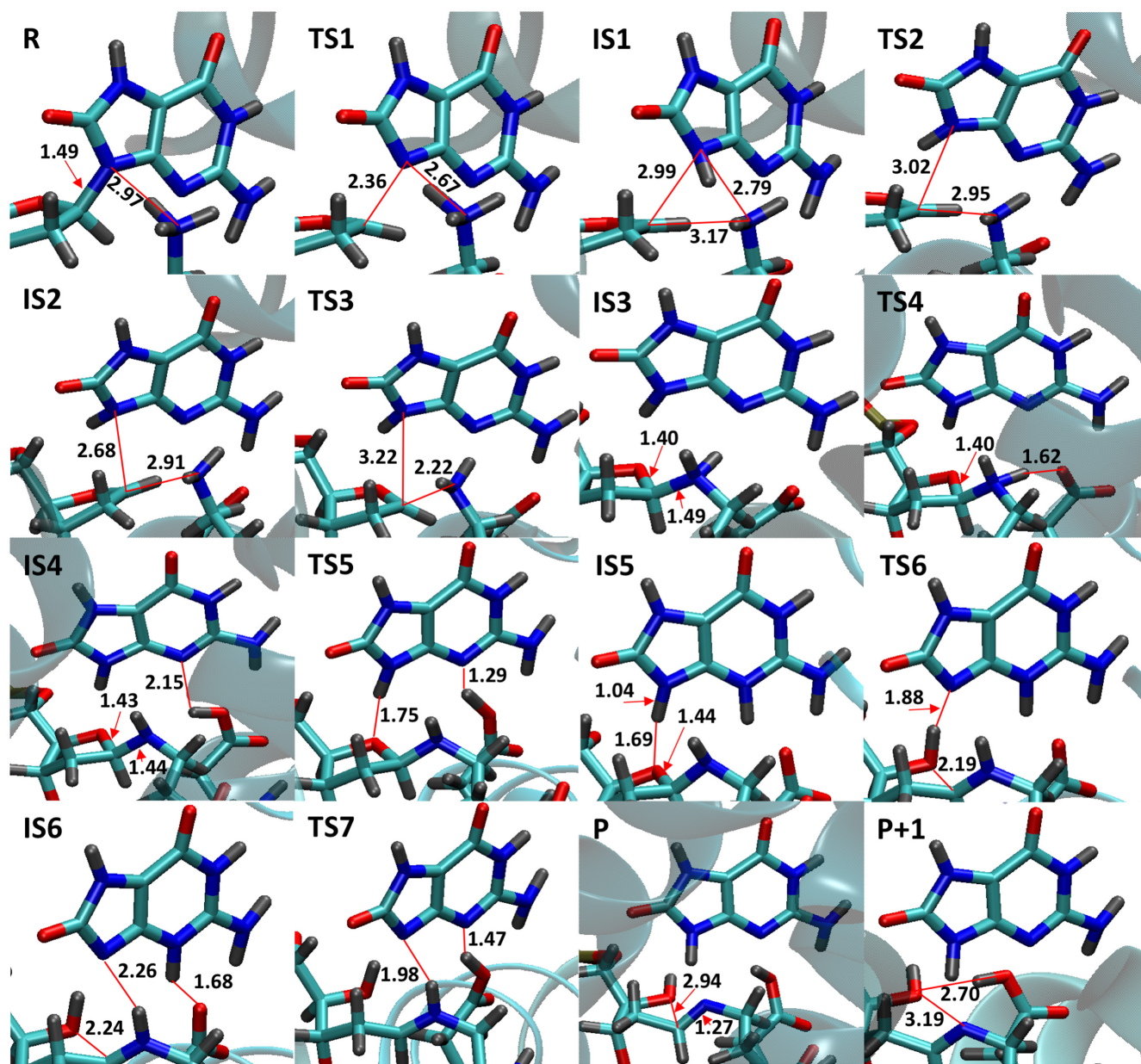
Figure 2. The local geometries of the catalytic core calculated for stationary states of the glycosylase reaction operated by hOGG1. The interatomic distances are in Å.

lase reaction captured in the 2NOZ and 1HU0 crystals. The rate-limiting step of the calculated glycosylase reaction was the formation of the Schiff base (TS6 and Figure 3). The formation of the Lys249–ribose covalent adduct (TS3) and the excision of the oxoG base (TS1) were similarly demanding. The Gibbs free activation energy, Gibbs free enthalpy and entropy calculated for the base excision were 16.1, 15.8 and −0.9 cal/K.mol, respectively. The calculated thermodynamic parameters associated with TS3 and TS6 states were similar: $\Delta G^{\#} = 16.2$ kcal/mol, $\Delta H^{\#} = 15.6$ kcal/mol, $\Delta S^{\#} = -2.1$ cal/K mol and $\Delta G^{\#} = 17.7$ kcal/mol, $\Delta H^{\#} = 17.0$ kcal/mol, $\Delta S^{\#} = -2.4$ cal/K mol (Supplementary Table S3). The activation energy, activation enthalpy and entropy measured for the glycosylase reaction with hOGG1

were 19.6, 18.6 kcal/mol and −3.5 cal/K mol, respectively (64). The QM/MM-calculated and measured thermodynamic parameters agreed well, which indicated the plausibility of the calculated reaction. The initial attack of the lone-pair from N9(oxoG) to NH_3^{+}(Lys249) was critical for the base-excision reaction. The N9(oxoG)•••H^{+}(Lys249) interaction was induced and energy-stabilized, mostly owing to the favorable arrangement of Lys249 within the catalytic core (63). The capacity of the glycosidic nitrogen N9 for accepting a proton from NH_3^{+}(Lys249) was conclusive for accelerating the oxoG excision. Nucleophilic character of the N9(oxoG) atom in the course of rupturing the N-glycosidic bond was illustrated with the Fukui function F^2. Nucleophilicity of the N9(oxoG) atom increased with elon-
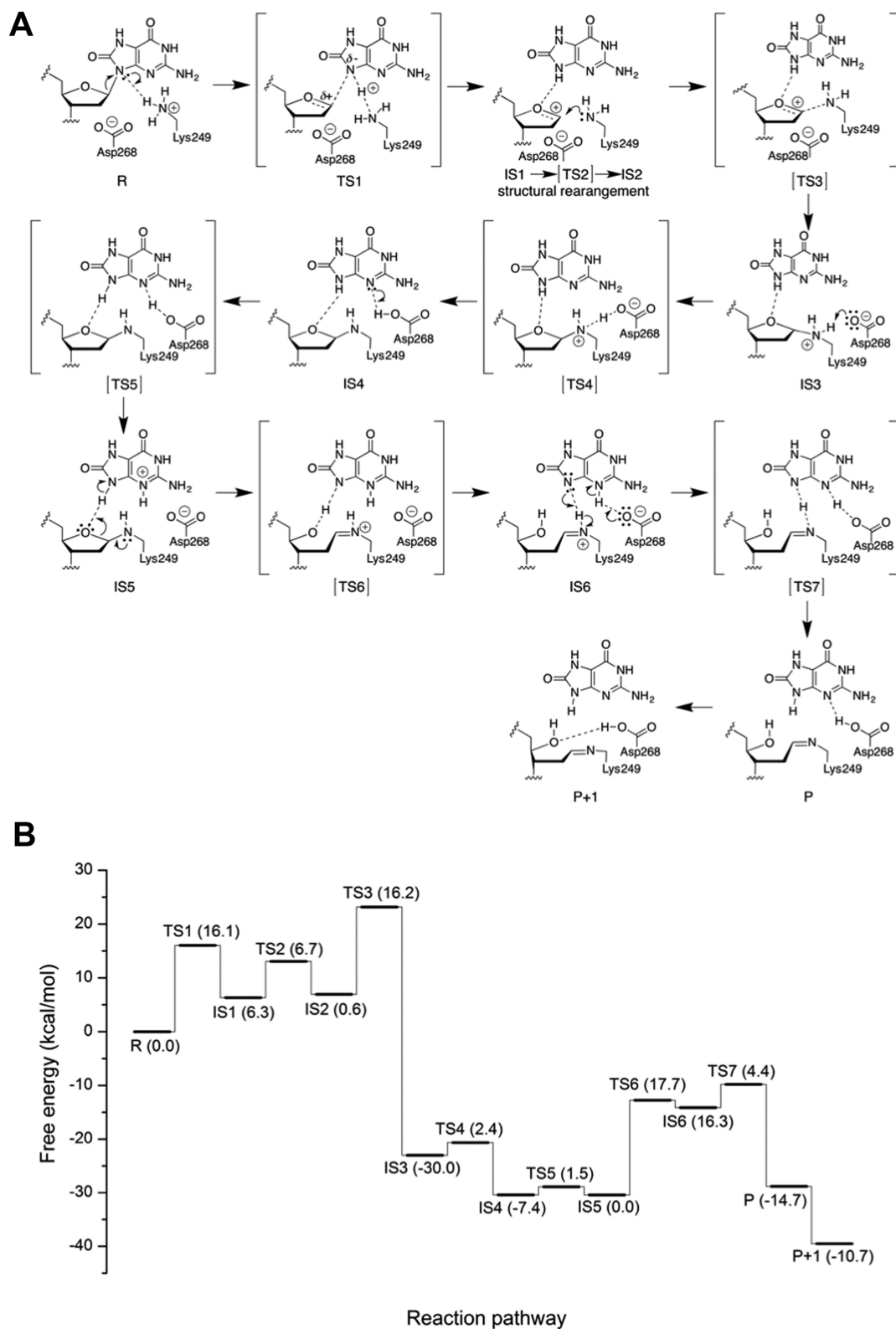
Figure 3. The chemical diagram (**A**) and free-energy profile (**B**) of the QM/MM-calculated glycosylase reaction with hOGG1. The Gibbs free energy profile included the following reaction steps: excision of the oxoG base (TS1), rearrangement of the catalytic core (TS2), formation of the Lys249–ribose covalent adduct (TS3), deprotonation of the Lys249–ribose adduct with $CO_2{}^-$(Asp268) (TS4), N3-protonation of the oxoG base (TS5), formation of the protonated Schiff base via opening of ribose ring of the Lys249–ribose adduct (TS6), deprotonation of the Schiff base via double proton transfer that resulted in product P (TS7) and rearrangement of the catalytic core particularly involving CO_2H(Asp268) (P+1). The Gibbs free activation and reaction energies in the parenthesis were referenced to the energies of the previous contiguous intermediate state.

gation of the N9-C1′ bond up to the TS1 state, which illustrated an increasing need for compensation of the negative charge on the oxoG base (Supplementary Figure S4). By contrast, the character of the C1′(ribose) atom was electroneutral and it switched abruptly to electrophilic only when the N9-C1′ bond ruptured (Supplementary Figure S5). The transfer of the proton from NH_3^+(Lys249) to N9(oxoG) was thus gradually enhanced during rupture of the C1′-N9 bond while the saturation of ribose oxocarbenium became critical only when the N-glycosidic bond ruptured.

The formation of a protonated Schiff base via opening of the ribose ring within the Lys249–ribose adduct (TS6) was the rate-limiting step of the calculated reaction (Figure 3). The opening of the ribose ring of the oxoG nucleoside was also the rate-limiting step of the Ribose-protonated base-excision mechanism that assumes the NH_2(Lys249) and CO_2H(Asp268) forms of the key catalytic residues (42). In the same work, the Ribose-protonated mechanism was compared with the N9-protonated mechanism that was mistakenly associated with the σ-bond substitution mechanism. In the concrete, the opening of the ribose ring by the force of CO_2H(Asp268) prior to excision of the oxoG base was con concluded to be the optimal catalytic strategy with hOGG1 (42). The Ribose-protonated mechanism was therefore compared with the true σ-bond substitution mechanism, and it was concluded that the plausibility of the true σ-bond substitution mechanism cannot be judged with calculations of the N9-protonated mechanism in Ref. (42), and the Ribose-protonated mechanism is unlikely ($\Delta G^\# = 42.2$ kcal/mol). The details can be found in the Supporting Theoretical Section.

^{1}H NMR monitoring of oxoG excision with WT hOGG1 and hOGG1(D268N)

The mutation of Asp268 to Asn corrupted the function of hOGG1 (32). The compensation of the developing charge at ribose oxocarbenium with Asn268 would be smaller compared to the effect of CO_2^-(Asp268) (Figure 1B). This assumption might explain the measured dysfunction of the hOGG1(D268N) mutant; however, the effect of Asn268 has not been explained. In particular, it remained unclear whether the glycosylase or subsequent β-lyase reaction was affected by the D268N mutation. This issue was resolved with the ^{1}H NMR spectroscopy monitoring of the catalytic activities of WT hOGG1 and the hOGG1(D268N) mutant.

At first, the catalytic activity of WT hOGG1 involving both the glycosylase and β-lyase reaction was examined based on the concept outlined in Figure 4A. The reaction yield employing WT hOGG1 was analyzed using a denaturing PAGE that demonstrated cleavage of the oxoG-containing DNA with the reaction products detected at the bottom (Figure 4B). By contrast, the activity of hOGG1(D268N) was not detected. Hence, the catalytic reaction with hOGG1(D268N) was blocked as was described already in Ref. (32). However, the experiment did not determine whether the glycosylase or β-lyase reaction was inhibited owing to the D268N mutation. The glycosylase reaction was therefore monitored with ^{1}H NMR spectroscopy. The oxoG-specific H7 NMR signal in the oxoG-containing DNA duplex at 10 ppm was used as a marker of the re-

action. The H7 signal was gradually reduced when WT hOGG1 was added, and after 20 h, it disappeared entirely owing to precipitation of the cleaved oxoG base (Figure 5B). By contrast, the H7 signal remained unaffected when hOGG1(D268N) was added, which clearly demonstrated loss of the base-excision function within glycosylase activity (Figure 5C). The non-enzymatic cleavage of oxoG did not occur (Figure 5D). The HSQC NMR spectra of hOGG1(D268N) and WT hOGG1 demonstrated the same folding for the two proteins (Supplementary Figure S6). Loss of the base-excision function for hOGG1(D268N) therefore occurred because of the D268N mutation.

QM/MM calculations of oxoG excision with hOGG1(D268 N) mutant

The optimized geometry of hOGG1(D268N) was similar to the geometry of WT hOGG1. The attack of lone pair electrons from N9(oxoG) to NH_3^+(Lys249) resulted in N9-pyramidalization of oxoG (Supplementary Table S9). However, the initial activation of the N-glycosidic bond was likely less effective. The C1′-N9 bond length was 1.469 Å, whereas that of WT hOGG1 was 1.493 Å. For protonated Asp268, the C1′-N9 bond length was 1.465 Å. The neutral charge of residue Asn268 thus affected the oxoG reactant unfavorably. The dependence of energy on the C1′-N9 distance further illustrated the effect of the charge of residue 268 on the activation energy of base-excision reaction (Supplementary Figure S3). The energy maxima for hOGG1(D268N) and hOGG1(CO_2H(Asp268)) were even larger than the energy maximum for the S_N1 mechanism where protonation of the departing base could not occur owing to the NH_2(Lys249) form. The $\Delta G^\#$ energy for oxoG excision with hOGG1(D268N) and hOGG1(CO_2H(Asp268)) was 28.7 and 26.9 kcal/mol, respectively. The effect of the CO_2^-(Asp268) carboxyl group on oxoG excision is clearly critical.

The electronic states of the N9 and C1′ atoms during oxoG excision were illustrated with F^2(N9) and F^2(C1′) Fukui indices. For WT hOGG1, nucleophilicity of the N9(oxoG) atom developed up to the TS1 state, whereas for hOGG1(D268N), the nucleophilic character of N9(oxoG) flipped to electrophilic long before TS1 (Supplementary Figure S4). The ability of the N9(oxoG) atom to accept the proton from NH_3^+(Lys249) was thus notably reduced by the D268N mutation. Both the mutation of Asp268 to Asn and protonation of Asp268 resulted more likely in an S_N1-like type of base-excision reaction (unsaturated leaving oxoG anion) despite favorable positioning and close proximity of NH_3^+(Lys249). The effects of CO_2^-(Asp268) and NH_3^+(Lys249) are therefore conjugated. CO_2^-(Asp268) compensates for the gradually vanishing C1′-N9 bond, while the Lys249 donates a proton at the most critical N9 atom of the departing oxoG base.

The principal effect of Asp268 on transfer of the proton from NH_3^+(Lys249) to N9(oxoG) was illustrated with the two-dimensional (2D) potential energy surfaces describing oxoG excision with WT hOGG1 and hOGG1(D268N) (Figure 6). The σ-bond substitution reaction with WT hOGG1 was associated with the lowest energy barrier on the 2D surface that connected the reactant with the IS1 sta-
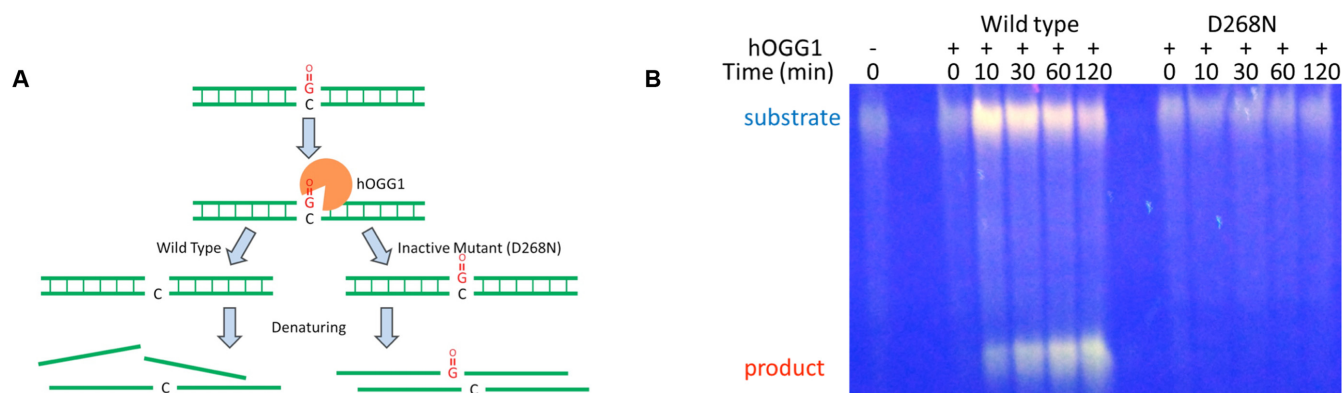
Figure 4. The catalytic function of WT hOGG1 and hOGG1(D268N). Concept of the assay for monitoring the enzymatic activity (**A**). Denaturing PAGE of the DNA duplex after processing with WT hOGG1 and hOGG1(D268N) (**B**). Details can be found in the Supporting Experimental Section.
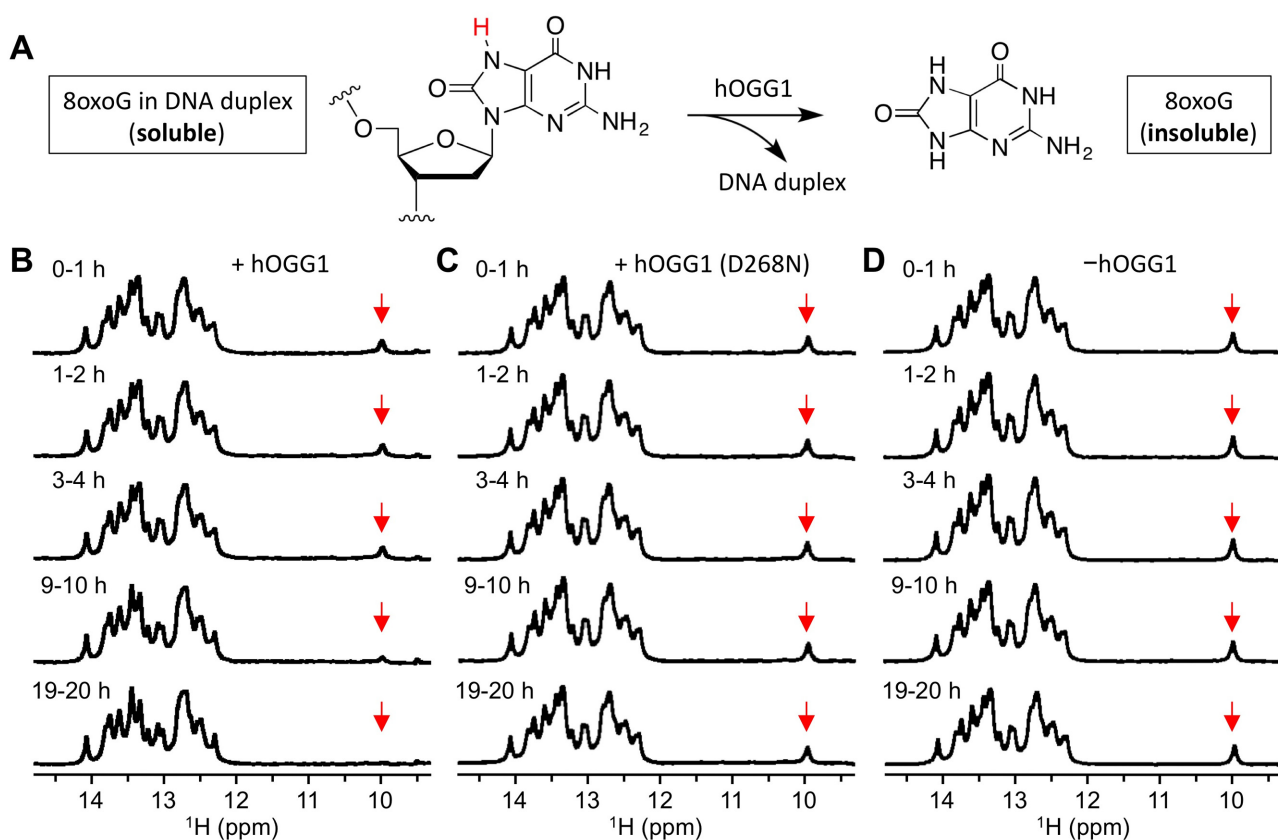

Figure 5. ^{1}H NMR monitoring of the base-excision reaction with WT hOGG1 and hOGG1(D268N) mutant. The glycosylase reaction for oxoG-containing DNA duplex was monitored with the ^{1}H NMR signal of the H7 proton of oxoG (red) at 10 ppm (**A**). ^{1}H NMR spectra in the presence of WT hOGG1 (**B**). ^{1}H NMR spectra in the presence of hOGG1(D268N) mutant (**C**). ^{1}H NMR spectra of the oxoG-containing DNA duplex only (**D**). Time course of the measurements in hours.

tionary state (Figure 6A). The excision of the oxoG base, where the transfer of the proton from NH_3^+(Lys249) to N9(oxoG) was blocked (the S_N1-like reaction), proceeded via a larger activation barrier that was similar to the activation barrier of the S_N1 reaction mechanism calculated with NH_2(Lys249) (Supplementary Figure S3). The low-energy area within the 2D potential surface indicated with the arrow for the S_N1-like reaction could include a stable reaction intermediate; however, optimization of the grid point

geometry with the lowest energy within that area (C1′-N9 = 2.30 Å, N9-H = 1.75 Å) without the geometric constraints resulted in an optimized reactant. Notable activation energies and unstable reaction products for the S_N1 reaction were also calculated previously (44,45). A lack of compensation of the negative charge on the departing oxoG base thus adversely affects both the activation barrier of base excision and stabilization of the reaction product. The mutation of Asp268 to Asn affected the 2D potential signif-
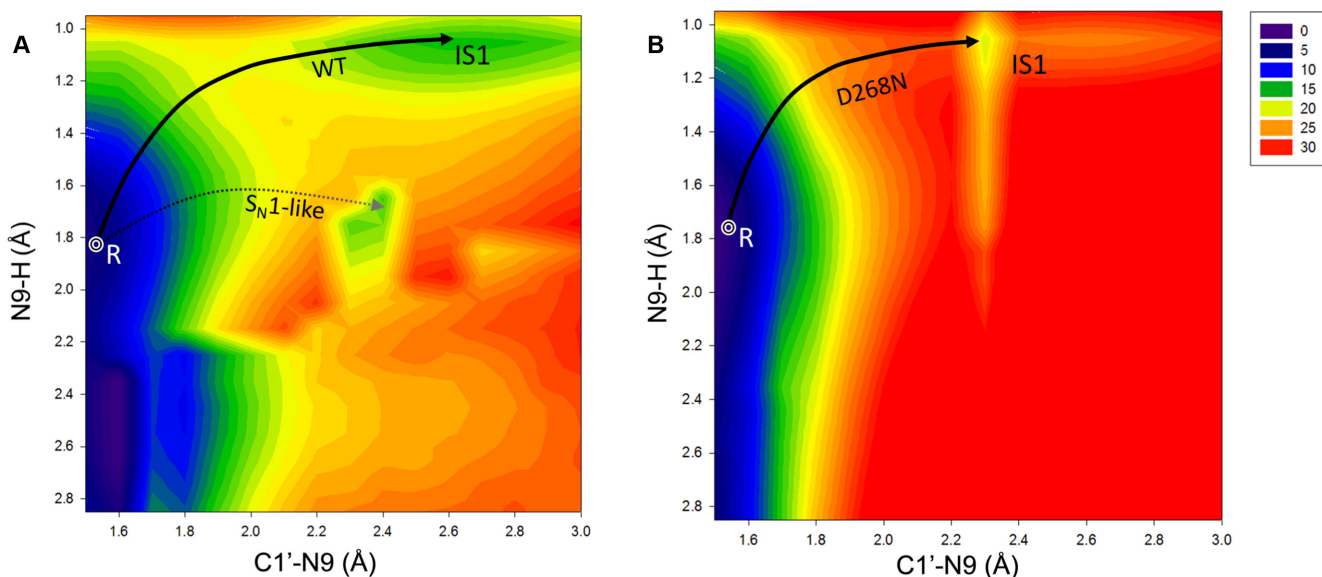
Figure 6. The QM/MM-calculated two-dimensional potential energy surfaces for excision of the oxoG base with WT hOGG1 (**A**) and hOGG1(D268N) mutant (**B**). The relative energies, with respect to the energy of reactant in kcal/mol, are indicated with different colors, as depicted in the right-upper box. N9-H is the distance between the N9(oxoG) atom and the interacting proton of NH_3^+(Lys249) group. C1′-N9 is the length of the N-glycosidic bond of oxoG. The relative energies were calculated employing the 0.1×0.1 Å geometric grid. Putative flow of the base-excision reactions discussed in the main text is indicated with arrows.

icantly (Figure 6B). The excision of the oxoG base with hOGG1(D268N) was practically precluded irrespective of whether the leaving oxoG base was protonated with Lys249. The effect of CO_2^-(Asp268) was therefore imperative for preserving the base-excision function of hOGG1.

DISCUSSION

The QM/MM-calculated reaction pathway connected the reactant of the glycosylase reaction closely before oxoG excision that was captured in the 2NOZ crystal with the reaction product that was captured in the 1HU0 crystal (Figure 1C and D). The geometry of the reduced form of the Schiff base in the 1HU0 crystal was similar to the QM/MM-calculated geometry of the Schiff base. The excision of the oxoG base, formation of the Lys249–ribose adduct and formation of the Schiff base were similarly demanding reaction steps (Figure 3). The formation of the Schiff base was nevertheless the rate-limiting step of the calculated glycosylase reaction. Stabilization of the excised oxoG base was calculated only after formation of the Lys249–ribose adduct. The glycosylase reaction was definitely stabilized by opening the ring of the Lys249–ribose covalent intermediate, that is, by formation of the Schiff base. The calculated $\Delta G^\#$ energies for the three reaction steps agreed with measured activation energies for the glycosylase reaction (Table 1). The calculated glycosylase reaction is therefore reliable with regard to Gibbs free energies and structures of the reactant and reaction product.

The BER enzymes can accelerate excision of damaged base in several ways (2–5) assuring thus ultimate biological role of the oxoG repair in cell, which was reviewed very recently (65). One particular way was illustrated for the oxoG excision with hOGG1 (Figure 7). The activa-

tion of the oxoG nucleoside within the catalytic core during breakage of the N-glycosidic bond simultaneously involved Lys249 and Asp268 for stabilization of the oxoG base anion and ribose oxocarbenium, respectively. NH_3^+(Lys249) epitomized 'reaction fuel' in the form of a proton that was captured by lone pair electrons at the glycosidic nitrogen and transferred to the N9(oxoG) atom in the course of base excision. CO_2^-(Asp268) epitomized 'reaction accelerator' by mimicking a virtual bond at C1′(ribose) during rupture of the N-glycosidic bond. Essential structural feature of the base-excision reaction was the pyramidal state of glycosidic nitrogen of oxoG substrate. The N9-pyramidalization was induced by residues of the catalytic site, particularly by the Lys249. The attack of lone pair electrons at N9(oxoG) to the proton of NH_3^+(Lys249) shifts electronic state of the pyramidal glycosidic nitrogen from sp^2-like toward sp^3-like, which triggers the substitution of N9-C1′ bond with an N9-H bond (46,63). The N9-pyramidalization of oxoG within hOGG1 catalytic core was induced likewise the N9-pyramidalization of G within the DNA G-quadruplex; i.e. by the molecular surroundings (66). The pyramidal geometry of glycosidic nitrogen was actually observed in the crystal structures of DNA and RNA molecules obtained at ultra-high resolution (67). Specific structural deformation of the damaged nucleobase operated by hOGG1 thus facilitated greatly the base-excision reaction, which initiated repair of the damaged DNA.

Lys249 and Asp268 are known to be indispensable for maintaining function of hOGG1. The significance of Asp268, which is a well-conserved residue within the OGG family of BER enzymes, was not clear (4). The particular effect of D268N mutation on the excision of the oxoG base was demonstrated experimentally (Figure 5) and rationalized theoretically (Figure 6); Asp268 is indispens-

Table 1. The Gibbs free activation energies in kcal/mol for the key steps of glycosylase reaction with WT hOGG1 and hOGG1(D268N) mutant

hOGG1	Residue 268	$\Delta G^{\#}$
Calculation: oxoG excision		
WT	CO_2^-(Asp)	16.1
WT	CO_2H(Asp)	26.9
D268N	$CONH_2$(Asn)	28.7
Calculation: lys249–ribose adduct		
WT	CO_2^-(Asp)	16.2
Calculation: schiff base		
WT	CO_2^-(Asp)	17.7
Experiment		
WT	Asp	19.6 [1]
WT	Asp	17.1 [2]
D268N	Asn	N.D. [3]

[1]Ref. (64).
[2]Refs. (45,68,69).
[3]Not determined (32).
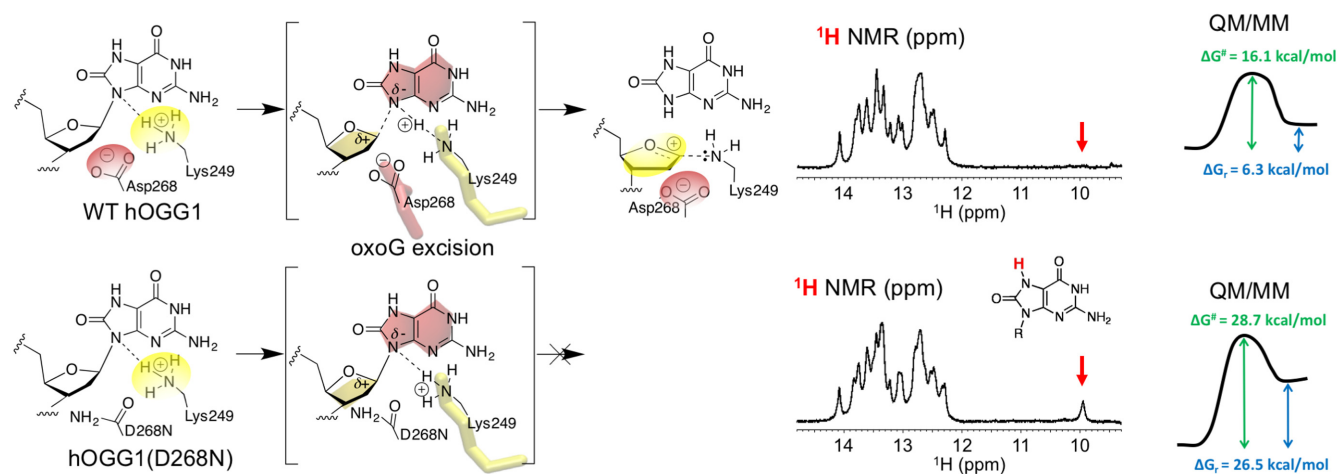
Figure 7. Summary for the base-excision reaction with hOGG1: compatibility of the charged residues within catalytic core was essential for the catalytic reaction, which was monitored for WT hOGG1 and hOGG1(D268N) mutant with NMR measurements, and loss of the base-excision function for the mutant was rationalized with the QM/MM-calculated $\Delta G^{\#}$ and ΔG_r energies.

able for maintaining the base-excision function of hOGG1. NMR monitoring of oxoG excision with WT hOGG1 and hOGG1(D268N) illustrated that the loss of the base-excision function when Asp268 was mutated to Asn occurred due to inadequate stabilization of ribose oxocarbenium. The QM/MM calculations illuminated that both the D268N mutation and the CO_2H(Asp268) form of Asp268 resulted in a notable increase in the activation barrier for oxoG excision (Table 1). The alternative Ribose-protonated mechanism that could employ CO_2H(Asp268) for opening of the ribose ring prior to oxoG excision is not likely to be not occurring (Supporting Theoretical Section). Moreover, the typical pKa value known for side-chain Asp indicates the CO_2^-(Asp268) form (47). Although the actual form of Asp268 in catalytically active hOGG1 is still not known, the σ-bond substitution reaction (TS1, Figure 3) can be currently regarded as a plausible base-excision reaction with hOGG1.

CONCLUSIONS

The glycosylase reaction carried out by the hOGG1 BER enzyme was studied with QM/MM calculations and NMR spectroscopy measurements of the catalytic function for WT hOGG1 and the hOGG1(D268N) mutant.

The excision of the oxoG base occurred via the NH_3^+(Lys249) and CO_2^-(Asp268) residues in a concerted manner that was complementary to the developing charges on the oxoG base and ribose during rupture of the N-glycosidic bond. Lys249 acts on the oxoG base as a proton-donating residue, whereas Asp268 acts on ribose as a charge-compensating residue. The Gibbs free activation energies calculated for the glycosylase reaction, including the excision of oxoG base and formation of the Lys249–ribose covalent adduct and Schiff base, were all smaller than 17.7 kcal/mol. The rate-limiting step of the glycosylase reaction was formation of the Schiff base by opening of the ribose ring within the Lys249–ribose covalent adduct. The breakdown of the base-excision function with the hOGG1(D268N) mutant was demonstrated with ^{1}H and ^{1}H-^{15}N HSQC NMR spectroscopy measurements and

rationalized with QM/MM calculations. The compensation of developing charges on the ribose oxocarbenium with the Asp268 carboxyl during oxoG excision was imperative to preserve the base-excision function of the hOGG1 BER enzyme.

SUPPLEMENTARY DATA

Supplementary Data are available at NAR Online.

REFERENCES

1. Lindahl,T. and Wood,R.D. (1999) Quality control by DNA repair. *Science*, **286**, 1897–1905.
2. David,S.S. and Wiliams,S.D. (1998) Chemistry of glycosylases and endonucleases involved in base-excision repair. *Chem. Rev.*, **98**, 1221–1261.
3. Stivers,J.T. and Jiang,Y.L. (2003) A mechanistic perspective on the chemistry of DNA repair glycosylases. *Chem. Rev.*, **103**, 2729–2759.
4. Berti,P.J. and McCann,J.A.B. (2006) Toward a detailed understanding of base excision repair enzymes: transition state and mechanistic analyses of N-glycoside hydrolysis and N-glycoside transfer. *Chem. Rev.*, **106**, 506–555.
5. David,S.S., O'Shea,V.L. and Kundu,S. (2007) Base-excision repair of oxidative DNA damage. *Nature*, **447**, 941–950.
6. Dodson,M.L., Michaels,M.L. and Lloyd,R.S. (1994) Unified catalytic mechanism for DNA glycosylases. *J. Biol. Chem.*, **269**, 32709–32712.
7. Wagenknecht,H.-A. (2006) The search for single DNA damage among millions of base pairs: DNA glycosylases trapped at work. *Angew. Chem. Int. Ed. Engl.*, **45**, 5583–5585.
8. Bruner,S.D., Norman,D.P.G. and Verdine,G.L. (2000) Structural basis for recognition and repair of the endogenous mutagen 8-oxoguanine in DNA. *Nature*, **403**, 859–866.
9. Rowland,M.M., Schonhoft,J.D., McKibbin,P.L., David,S.S. and Stivers,J.T. (2014) Microscopic mechanism of DNA damage searching by hOGG1. *Nucleic Acids Res.*, **42**, 9295–9303.
10. Paz-Elizur,T., Sevilya,Z., Leitner-Dagan,Y., Elinger,D., Roisman,L.C. and Livneh,Z. (2008) DNA repair of oxidative DNA damage in human carcinogenesis: potential application for cancer risk assessment and prevention. *Cancer Lett.*, **266**, 60–72.
11. Kryston,T.B., Georgiev,A.B., Pissis,P. and Georgakilas,A.G. (2011) Role of oxidative stress and DNA damage in human carcinogenesis. *Mutat. Res.*, **711**, 193–201.
12. Dumont,H., Grber,R., Bignon,E., Morell,C., Aranda,J., Ravanat,J.-L. and Tunon,I. (2016) Singlet oxygen attack on guanine: reactivity and structural signature within the B-DNA helix. *Chemistry*, **22**, 1–6.
13. Hainaut,P., Hernandez,T., Robinson,A., Rodriguez-Tome,P., Flores,T., Hollstein,M., Harris,C.C. and Montesano,R. (1998) IARC database of p53 gene mutations in human tumors and cell lines: updated compilation, revised formats and new visualisation tools. *Nucleic Acids Res.*, **26**, 205–213.
14. Helleday,T., Petermann,E., Lundin,C., Hodgson,B. and Sharma,R.A. (2008) DNA repair pathways as targets for cancer therapy. *Nat. Rev. Cancer*, **8**, 193–204.
15. Lu,R.Z., Nash,H.M. and Verdine,G.L. (1997) A mammalian DNA repair enzyme that excises oxidatively damaged guanines maps to a locus frequently lost in lung cancer. *Curr. Biol.*, **7**, 397–407.
16. Arai,K., Morishita,K., Shinmura,K., Kohno,T., Kim,S.R., Nohmi,T., Taniwaki,M., Ohwada,S. and Yokota,J. (1997) Cloning of a human homolog of the yeast OGG1 gene that is involved in the repair of oxidative DNA damage. *Oncogene*, **14**, 2857–2861.
17. Roldan-Arjona,T., Wei,Y.F., Carter,K.C., Klungland,A., Anselmino,C., Wang,R.P., Augustus,M. and Lindahl,T. (1997) Molecular cloning and functional expression of a human cDNA encoding the antimutator enzyme 8-hydroxyguanine-DNA glycosylase. *Proc. Natl. Acad. Sci. U.S.A.*, **94**, 8016–8020.
18. Bjoras,M., Luna,L., Johnson,B., Hoff,E., Haug,T., Rognes,T. and Seeberg,E. (1997) Opposite base-dependent reactions of a human base excision repair enzyme on DNA containing 7,8-dihydro-8-oxoguanine and abasic sites. *EMBO J.*, **16**, 6314–6322.
19. Rosenquist,T.A., Zharkov,D.O. and Grollman,A.P. (1997) Cloning and characterization of a mammalian 8-oxoguanine DNA glycosylase. *Proc. Natl. Acad. Sci. U.S.A.*, **94**, 7429–7434.
20. Radicella,J.P., Dherin,C., Desmaze,C., Fox,M.S. and Boiteux,S. (1997) Cloning and characterization of hOGG1, a human homolog of the OGG1 gene of Saccharomyces cerevisiae. *Proc. Natl. Acad. Sci. U.S.A.*, **94**, 8010–8015.
21. Kuo,F.C. and Sklar,J. (1997) Augmented expression of a human gene for 8-oxoguanine DNA glycosylase (MutM) in B lymphocytes of the dark zone in lymph node germinal centers. *J. Exp. Med.*, **186**, 1547–1556.
22. Aburatani,H., Hippo,Y., Ishida,T., Takashima,R., Matsuba,C., Kodama,T., Takao,M., Yasui,A., Yamamoto,K., Asano,M. *et al.* (1997) Cloning and characterization of mammalian 8-hydroxyguanine-specific DNA glycosylase/apurinic, apyrimidinic lyase, a functional mutM homologue. *Cancer Res.*, **57**, 2151–2156.
23. Nash,H.M., Bruner,S.D., Scharer,O.D., Kawate,T., Addona,T.A., Sponner,E., Lane,W.S. and Verdine,G.L. (1996) Cloning of a yeast 8-oxoguanine DNA glycosylase reveals the existence of a base-excision DNA-repair protein superfamily. *Curr. Biol.*, **6**, 968–980.
24. Boiteux,S. and Radicella,J.P. (2000) The human OGG1 gene: Structure, functions, and its implication in the process of carcinogenesis. *Arch. Biochem. Biophys.*, **377**, 1–8.
25. Banerjee,A., Yang,W., Karplus,M. and Verdine,G.L. (2005) Structure of a repair enzyme interrogating undamaged DNA elucidates recognition of damaged DNA. *Nature*, **434**, 612–618.
26. Hamm,M.L., Gill,T.J., Nicolson,S.C. and Summers,M.R. (2007) Substrate specificity of fpg (MutM) and hOGG1, two repair glycosylases. *J. Am. Chem. Soc.*, **129**, 7724–7725.
27. McKibbin,P.L., Kobori,A., Taniguchi,Y., Kool,E.T. and David,S.S. (2012) Surprising repair activities of nonpolar analogs of 8-oxoG expose features of recognition and catalysis by base excision repair glycosylases. *J. Am. Chem. Soc.*, **134**, 1653–1661.
28. Yin,Y.Z., Sasaki,S. and Taniguchi,Y. (2015) Recognition and excision properties of 8-halogenated-7-deaza-2-deoxyguanosine as 8-oxo-2-deoxyguanosine analogues and Fpg and hOGG1 inhibitors. *Chembiochem*, **16**, 1190–1198.
29. Crenshaw,C.M., Kwangho,N., Kimberly,O., Kutchikian,P.S., Bowman,B., Karplus,M. and Verdine,G.L. (2012) Enforced presentation of an extrahelikal guanine to the lesion recognition pocket of human 8-oxoguanine glycosylase, hOGG1. *J. Biol. Chem.*, **287**, 24916–24928.
30. Lee,S., Radom,C.T. and Verdine,G.L. (2008) Trapping and structural elucidation of a very advanced intermediate in the lesion-extrusion pathway of hOGG1. *J. Am. Chem. Soc.*, **130**, 7784–7785.
31. Donley,N., Jaruga,P., Coskun,E., Dizdaroglu,M., McCullough,A.K. and Lloyd,R.S. (2015) Small molecule inhibitors of 8-oxoguanine DNA glycosylase-1 (OGG1). *ACS Chem. Biol.*, **10**, 2334–2343.
32. Norman,D.P.G., Chung,S.J. and Verdine,G.L. (2003) Structural and biochemical exploration of a critical amino acid in human 8-oxoguanine glycosylase. *Biochemistry*, **42**, 1564–1572.
33. Radom,C.T., Banerjee,A. and Verdine,G.L. (2007) Structural characterization of human 8-oxoguanine DNA glycosylase variants bearing active site mutations. *J. Biol. Chem.*, **282**, 9182–9194.
34. Fromme,J.C., Bruner,S.D., Yang,W., Karplus,M. and Verdine,G.L. (2003) Product-assisted catalysis in base-excision DNA repair. *Nat. Struct. Mol. Bio.*, **10**, 204–211.
35. Norman,D.P.G., Bruner,S.D. and Verdine,G.L. (2001) Coupling of substrate recognition and catalysis by a human base-excision DNA repair protein. *J. Am. Chem. Soc.*, **123**, 359–360.

36. Kow,Y.W. and Wallace,S.S. (1987) Mechanism of action of escherichia-coli endonuclease-III. *Biochemistry*, **26**, 8200–8206.

37. Nash,H.M., Lu,R.Z., Lane,W.S. and Verdine,G.L. (1997) The critical active-site amine of the human 8-oxoguanine DNA glycosylase, hOGG1: direct identification, ablation and chemical reconstitution. *Chem. Biol.*, **4**, 693–702.

38. Warshel,A., Sharma,P.K., Kato,M., Xiang,Y., Liu,H.B. and Olsson,M.H.M. (2006) Electrostatic basis for enzyme catalysis. *Chem. Rev.*, **106**, 3210–3235.

39. Shim,E.J., Przybylski,J.L. and Wetmore,S.D. (2010) Effects of nucleophile, oxidative damage, and nucleobase orientation on the glycosidic bond cleavage in deoxyguanosine. *J. Phys. Chem. B*, **114**, 2319–2326.

40. Kellie,J.L., Wilson,K.A. and Wetmore,S.D. (2015) An ONIOM and MD investigation of possible monofunctional activity of human 8-oxoguanine-DNA glycosylase (hOGG1). *J. Phys. Chem. B*, **119**, 8013–8023.

41. Osakabe,T., Fujii,Y., Hata,M., Tsuda,M., Neya,S. and Hoshino,T. (2004) Quantum chemical study on base excision mechanism of 8-oxoguanine DNA glycosylase. *Chem. Bio Inform. J.* **4**, 73–92.

42. Sadeghian,K. and Ochsenfeld,C. (2015) Unraveling the base excision repair mechanism of human DNA glycosylase. *J. Am. Chem. Soc.*, **137**, 9824–9831.

43. Fromme,J.C. and Verdine,G.L. (2003) Structure of a trapped endonuclease III-DNA covalent intermediate. *EMBO J.*, **22**, 3461–3471.

44. Schyman,P., Danielsson,J., Pinak,M. and Laaksonen,A. (2005) Theoretical study of the human DNA repair protein hOGG1 activity. *J. Phys. Chem. A*, **109**, 1713–1719.

45. Calvaresi,M., Bottoni,A. and Garavelli,M. (2007) Computational clues for a new mechanism in the glycosylase activity of the human DNA repair protein hOGG1. A generalized paradigm for purine-repairing systems? *J. Phys. Chem. B*, **111**, 6557–6570.

46. Šebera,J., Trantírek,L., Tanaka,Y. and Sychrovský,V. (2012) Pyramidalization of the glycosidic nitrogen provides the way for efficient cleavage of the N-glycosidic bond of 8-oxoG with the hOGG1 DNA repair protein. *J. Phys. Chem. B*, **116**, 12535–12544.

47. Pace,C.N., Grimsley,G.R. and Scholtz,J.M. (2009) Protein ionizable groups: pK values and their contribution to protein stability and solubility. *J. Biol. Chem.*, **284**, 13285–13289.

48. Tanaka,Y., Yamaguchi,H., Oda,S., Kondo,Y., Nomura,M., Kojima,C. and Ono,A. (2006) NMR spectroscopic study of a DNA duplex with mercury-mediated T-T base pairs. *Nucleosides Nucleotides Nucleic Acids*, **25**, 613–624.

49. Tanaka,Y., Oda,S., Yamaguchi,H., Kondo,Y., Kojima,C. and Ono,A. (2007) N-15-N-15 J-coupling across Hg-II: direct observation of Hg-II-mediated T-T base pairs in a DNA duplex. *J. Am. Chem. Soc.*, **129**, 244–245.

50. Uchiyama,T., Miura,T., Takeuchi,H., Dairaku,T., Komuro,T., Kawamura,T., Kondo,Y., Benda,L., Sychrovský,V., Bouř,P. *et al.* (2012) Raman spectroscopic detection of the T-Hg-II-T base pair and the ionic characteristics of mercury. *Nucleic Acids Res.*, **40**, 5766–5774.

51. Dairaku,T., Furuita,K., Sato,H., Kondo,Y., Kojima,C., Ono,A. and Tanaka,Y. (2015) Exploring a DNA sequence for the three-dimensional structure determination of a silver(I)-mediated C-C base pair in a DNA duplex by H-1 NMR spectroscopy. *Nucleosides Nucleotides Nucleic Acids*, **34**, 877–900.

52. Zhao,Y. and Truhlar,D.G. (2008) The M06 suite of density functionals for main group thermochemistry, thermochemical kinetics, noncovalent interactions, excited states, and transition elements: two new functionals and systematic testing of four

53. Harihara,P.C. and Pople,J.A. (1973) Influence of polarization functions on molecular-orbital hydrogenation energies. *Theor. Chim. Acta*, **28**, 213–222.

54. Banks,J.L., Beard,H.S., Cao,Y.X., Cho,A.E., Damm,W., Farid,R., Felts,A.K., Halgren,T.A., Mainz,D.T., Maple,J.R. *et al.* (2005) Integrated modeling program, applied chemical theory (IMPACT). *J. Comput. Chem.*, **26**, 1752–1780.

55. (2013) *Jaguar, v. 8.2, Schrödinger.* LLC, NY.

56. Bochevarov,A.D., Harder,E., Hughes,T.F., Greenwood,J.R., Braden,D.A., Philipp,D.M., Rinaldo,D., Halls,M.D., Zhang,J. and Friesner,R.A. (2013) Jaguar: a high-performance quantum chemistry software program with strengths in life and materials sciences. *Int. J. Quantum Chem.*, **113**, 2110–2142.

57. (2013) *Impact, v. 6.1, Schrödinger.* LLC, NY.

58. (2013) *QSite, v. 6.1, Schrödinger.* LLC, NY.

59. Friesner,R.A. and Guallar,V. (2005) Ab initio quantum chemical and mixed quantum mechanics/molecular mechanics (QM/MM) methods for studying enzymatic catalysis. *Annu. Rev. Phys. Chem.*, **56**, 389–427.

60. Contreras,R.R., Fuentealba,P., Galvan,M. and Perez,P. (1999) A direct evaluation of regional fukui functions in molecules. *Chem. Phys. Lett.*, **304**, 405–413.

61. Morell,C., Grand,A. and Toro-Labbe,A. (2005) New dual descriptor for chemical reactivity. *J. Phys. Chem. A*, **109**, 205–212.

62. Chamorro,E. and Perez,P. (2005) Condensed-to-atoms electronic Fukui functions within the framework of spin-polarized density-functional theory. *J. Chem. Phys.*, **123**, 114107.

63. Šebera,J., Trantírek,L., Tanaka,Y., Nencka,R., Fukal,J. and Sychrovský,V. (2014) The activation of N-glycosidic bond cleavage performed by base-excision repair enzyme hOGG1; theoretical study of the role of Lys 249 residue in activation of G, OxoG and FapyG. *RSC Adv.*, **4**, 44043–44051.

64. Kuznetsov,N.A., Kuznetsova,A.A., Vorobjev,Y.N., Krasnoperov,L.N. and Fedorova,O.S. (2014) Thermodynamics of the DNA damage repair steps of human 8-oxoguanine DNA glycosylase. *PLoS One*, **9**, e98495.

65. Boiteux,S., Coste,F. and Castaing,B. (2016) Repair of 8-oxo-7,8-dihydroguanine in prokaryotic and eukaryotic cells: properties and biological roles of the Fpg and OGG1 DNA N-glycosylases. *Free Radic. Biol. Med.*, doi:10.1016 /j.freeradbiomed.11.042.

66. Sychrovský,V., Vokáčová,Z.S. and Trantírek,L. (2012) Guanine bases in DNA G-quadruplex adopt nonplanar geometries owing to solvation and base pairing. *J. Phys. Chem. A*, **116**, 4144–4151.

67. Sychrovský,V., Foldynová-Trantírková,S., Špačková,N., Robeyns,K., Van Meervelt,L., Blankenfeldt,W., Vokáčová,Z., Šponer,J. and Trantírek,L. (2009) Revisiting the planarity of nucleic acid bases: pyramidilization at glycosidic nitrogen in purine bases is modulated by orientation of glycosidic torsion. *Nucleic Acids Res.*, **37**, 7321–7331.

68. Vidal,A.E., Hickson,I.D., Boiteux,S. and Radicella,J.P. (2001) Mechanism of stimulation of the DNA glycosylase activity of hOGG1 by the major human AP endonuclease: bypass of the AP lyase activity step. *Nucleic Acids Res.*, **29**, 1285–1292.

69. Hill,J.W., Hazra,T.K., Izumi,T. and Mitra,S. (2001) Stimulation of human 8-oxoguanine-DNA glycosylase by AP-endonuclease: potential coordination of the initial steps in base excision repair. *Nucleic Acids Res.*, **29**, 430–438.

M06-class functionals and 12 other functionals. *Theor. Chem. Acc.*, **120**, 215–241.